A Dynamic Power Transfer Route Construction and Optimization Method Considering Random Node Distribution for Wireless Power Transfer Network

Jinde Wu, Yanling Li, Xin Dai, *Member, IEEE*, Ruozhong Gao, *Student Member, IEEE*, and Miao He, *Senior Member, IEEE*

***Abstract*—Wireless power transfer network (WPTN) is composed of nodes and power transfer routes, which can supply power for group devices. In the WPTN, it is difficult to build a definite power transfer route under the random node distribution condition. In this article, a dynamical construction and optimization strategy of power transfer route is proposed to adapt to random node distribution. In order to establish a definite route among grouping nodes, each node is designed to switch its role flexibly through a topology switching method. Furthermore, in the switching process of power transfer route, the switching method of node role shows that the transition is smooth. Then, an actual WPTN with five randomly distributed nodes verifies the effectiveness of the proposed method.**

***Index Terms*—Node role switching, power transfer route optimization, wireless power transfer network (WPTN).**

I. Introduction

OWING to the advantages in convenience, safety, and flexibility, wireless power transfer network (WPTN) has been widely used in household appliances [1], unmanned aerial vehicles (UAVs) [2], wearable devices [3], electric vehicles, moving robots [4], [5], etc. Cho et al. [1] showed the application of WPTN in household appliances. They propose a methodology for the design of WPT resonators that can achieve optimum efficiency for multiple receivers with power distribution ratios, loads, and distances. The system includes multiple repeaters, and each of them is connected to a resistive load. Each receiver transfers power to an adjacent receiver and acts as a relay while its load consumes power. The application of WPTN in UAV is shown in [2]. In [2], an optimal design process is proposed for the domino WPT system (similar to WPTN), which is able to charge the battery of an UAV from the high-voltage transmission line. The optimal design process is essential to provide the nominal charging power to the UAV's battery while maximizing the power transfer efficiency, respecting the zero-voltage switching of the power electronic switches and the space limitations of the coils. WPTN can also be used in wearable devices. A wearable system that is capable of tracking finger motion and recognizing a set of hand gestures is presented in [3]. A relay-resonator configuration is employed to provide a homogeneous magnetic field in the system. The WPTN proposed in [4] and [5] is applied in electric vehicle and moving robot. In these papers, a controllable power division method has been proposed and generalized among arbitrary number of receivers and repeaters.

In the WPTN, since the position of each device is random and dynamic, the power transfer route should also be changed accordingly. However, because of the cross coupling among devices, it is difficult to transfer power through the definite route. If a definite power transfer route can be built between the power source node and the receiver node, and the role of each node can be changed dynamically, it will achieve the practical applications of WPTN.

There are some relevant papers about wireless power transfer through the repeaters. Generally, in the previous studies, the repeaters can be added between the transmitter and the receiver to increase the transfer distance [6], enhance the transfer power and efficiency [7], and improve the system performance [8]. Zhang et al. [9] adopted multiple loads of resonant wireless power transmission. With the addition of the load coil, the three-coil structure has easy access to transfer power to multiple loads with the advantages of compact structure and controllable power flow. *LCC* topology is used in [10]. Constant voltage outputs can be obtained for all the loads, which facilitate the independent load power control. Zhong and Hui [11] proposed a multifrequency WPT system in which the power can be transferred from the transmitter to the targeted loads with receiver coils specifically tuned for power reception. In order to

Manuscript received 24 June 2023; revised 17 November 2023; accepted 21 December 2023. Date of publication 29 December 2023; date of current version 16 February 2024. This work was supported in part by the research funds for the National Natural Science Foundation of China under Grant 51977178, in part by the Fundamental Research Funds for the Central Universities under Grants 2022CDJQY-006 and 2021CDJXXXB002, and in part by the China National Center for International Research on Wireless Power Transfer Technologies. Recommended for publication by Associate Editor F. COSTA. *(Corresponding author: Yanling Li.)*

Jinde Wu is with the School of Electrical and Power Engineering, Taiyuan University of Technology, Shanxi 030024, China (e-mail: wujinde@tyut.edu.cn).

Yanling Li is with the School of Electrical Engineering and Electronic Information, Xihua University, Sichuan 610039, China (e-mail: yanling.li@mail.xhu.edu.cn).

Xin Dai and Ruozhong Gao are with the School of Automation, Chongqing University, Chongqing 400044, China (e-mail: daixin@cqu.edu.cn; gaoruozhong@cqu.edu.cn).

Miao He is with the Department of Electrical and Computer Engineering, Texas Tech University, Lubbock, TX 79401 USA (e-mail: miao.he@ttu.edu).

Color versions of one or more figures in this article are available at https://doi.org/10.1109/TPEL.2023.3348103.

Digital Object Identifier 10.1109/TPEL.2023.3348103

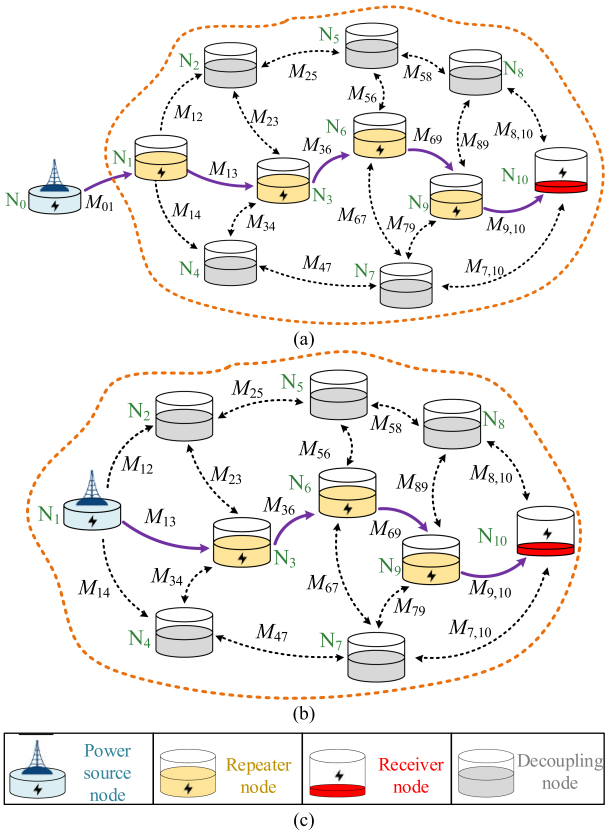

Fig. 1. Two different WPTN. (a) Active injection WPTN, (b) power autonomy injection WPTN, and (c) different node roles.

maintain constant transfer power and keep near-unity transfer efficiency at varying transfer distances, Shu et al. [12] proposed a WPT system with multiple repeaters based on the concept of parity-time symmetry. In addition to achieving constant output power, the transfer efficiency can be against the variation of the transfer distance without any tuning or feedback within a certain distance. In [13], an analysis method based on the quadratic eigenvalue problem is proposed for multirelay WPT system. The analytical solutions of currents induced in each coil are expressed in terms of the eigensolution. The authors in [14] and [15] studied the domino WPT system with coaxial and noncoaxial axes. An optimization method with multiple power flow paths is proposed by analyzing the noncoaxial domino WPT system. The mathematical expression for the power transfer efficiency with an optimal load is derived in [16] to improve the power transfer efficiency, and it also analyzes the effects of the varying repeater numbers on the power transfer efficiency. It confirms that there is an optimal repeater number for maximizing the achievable power transfer efficiency for a given end-to-end distance. Wu et al. [17] proposed a bidirectional multistage wireless power transfer method for robot arm that can provide power for multiple loads. A bowl-coupling structure and 3-D orthogonal ring coil arrangement are proposed to reduce coupling variation against joint rotation. With a special resonant topology design for each stage, energy can be injected or output freely on each stage regardless of energy transfer direction. This topology can also reduce the sensitivity of the output voltages with the load variation. For multinode WPT system, Wu et al. [18] proposed a flexible repeater power transfer mode characterized by node-role-change function. Each node role can be flexibly switched among repeater, receiver, and decoupling node through a topology switching method to satisfy dynamical repeater power transfer requirements. Graph sets method is proposed in [19] to model, analyze, and simplify the multicoil wireless power transfer system, and a set of rules are developed to analyze some important aspects.

The above research works mainly focus on system performance improvement by adding multiple repeaters. However, since each node role is a pre-set, so power transfer route across multiple nodes is normally fixed and cannot be changed dynamically. Therefore, the above repeaters' working modes cannot support the WPTN operations, which will limit WPT technology applications for group electronic devices.

In order to satisfy power transfer among group multiple devices (nodes), this article proposes a dynamic power transfer route construction and optimization method considering random node distribution for WPTN. The power transfer route can be changed dynamically according to node distribution. According to power transfer route requirement, each node can adjust its role correspondingly through topology switching method between the repeater and decoupling. This method increases the flexibility in group device charging and helps to set up a more reliable wireless power route to extend effective wireless power transfer distance. Finally, the simulation and experimental results verify that in the process of power transfer route switching, the switching transition is smooth.

II. Wireless Power Transfer Network

This article proposes a WPTN with multiple wireless power transfer electronic devices (nodes). The power can be transferred through the routes that are built among the devices. According to different application requirements, WPTN is divided into active injection WPTN [see Fig. 1(a)] and power autonomy injection WPTN [see Fig. 1(b)].

The active injection WPTN is shown in Fig. 1(a), where the system is injected with power from an external power source node. When the external power source node is connected to the WPTN, the power transfer route from the node to the receiver node is built, the relevant nodes in the network act as repeater nodes, and other nodes are decoupled, thus realizing the power supply to the receiver node.

The power autonomy injection WPTN is shown in Fig. 1(b). It is similar to the active injection mode, while the main difference is that there is no external power injection source. In the power autonomy injection WPTN, only the internal nodes with sufficient energy are used to transfer power to other nodes to satisfy the power supply of the receiver node.

In order to satisfy different power transfer requirements, the nodes can be divided as power source node, repeater node, receiver node, and decoupling node, are given as follows.

1) Power source node provides power source for WPTN.
2) Repeater node extends the area of WPTN and does not consume power.

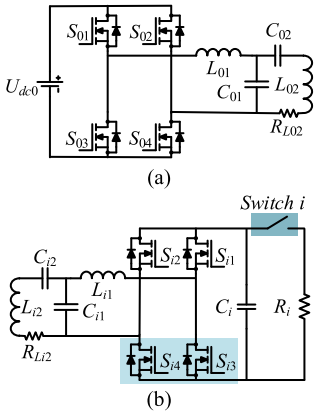

Fig. 2. Circuit models of different nodes. (a) Power source node. (b) Other nodes.

3) Receiver node actually consumes power.
4) Decoupling node does not participate in the power transfer.

The circuit models of different nodes are designed in Fig. 2. In order to achieve different objectives of power transfer, each node can switch its role according to different power transfer routes. This article proposes a topology switching method to change the role of nodes, and the topology model is shown in Fig. 2(b).

To analyze the system, some basic definitions are given as follows. As can be seen in Fig. 2(a), the power source node is composed of a power supply ($U_{\rm dc0}$), a full-bridge inverter (S_{01}–S_{04}), and a resonance compensation network (L_{01}-C_{01}-C_{02}-L_{02}). Other nodes shown in Fig. 2(b) are composed of a resonance compensation network (L_{i1}-C_{i1}-C_{i2}-L_{i2}), a full-bridge converter (S_{i1}-S_{i4}), a switch (*Switch i*), a filter capacitor (C_i), and a load (R_i). The resistance of each coil is expressed as R_{Li2}, and the equivalent ac impedance of the receiver node is expressed as R_{li}. The operation frequency of the inverter in power source node is f, and its angular frequency is ω ($\omega = 2\pi f$). The mutual inductance between N_i and N_j is expressed as M_{ij}.

The relationship between the dc voltage $U_{\rm dc0}$ and inverter output voltage $U_{\rm ac0}$ is

$$U_{\rm ac0} = \frac{2\sqrt{2}U_{\rm dc0}}{\pi}. \tag{1}$$

In the designed node topology. as shown in Fig. 2(b), the impedance Z_i of N_i can be expressed as

$$Z_i = R_{Li2} + j\omega L_{i2} + \frac{1}{j\omega C_{i2}} + \left(\frac{1}{j\omega C_{i1}} // \left(R_{li} + j\omega L_{i1}\right)\right). \tag{2}$$

Under the condition that the capacitances and inductances of each node satisfy (3) and (4), (2) can be simplified as (5)

$$\omega^2 = \frac{1}{L_{i1}C_{i1}} \ (i = 0, 1 \ldots n) \tag{3}$$

where

$$\frac{1}{j\omega C_{i2}} + j\omega L_{i2} = j\omega L_{i1} \tag{4}$$

$$Z_i = R_{Li2} + j\omega L_{i1} + \left(\frac{1}{j\omega C_{i1}} // \left(R_{li} + j\omega L_{i1}\right)\right)$$

$$= R_{Li2} + \frac{\left(\omega L_{i1}\right)^2}{R_{li}}. \tag{5}$$

It can be seen from (5) that when the capacitances and inductances of each node satisfy (3) and (4), the equivalent impedances of each node exhibit resistive.

As can be seen in Fig. 2(b), when *Switch i* is turned OFF, the node is a L_{i2}-C_{i1}-C_{i2}-R_{Li2} topology in series. According to (3) and (4), the node is still in resonant state. When S_{i3} and S_{i4} of the converter are turned ON, the load is short-circuited.

III. Construction and Optimization of Power Transfer Route

In the WPTN, it is necessary to transfer power from the power source node to the target receiver node through the optimal route. Under the condition that the position of each node is random and dynamic, the goal of power transfer in WPTN is to find the route with maximum efficiency. In this article, active injection WPTN with single power source node and single receiver node are taken as an example to study the construction and optimization of power transfer route. A node role switching method is introduced in detail. Furthermore, a power transfer route optimization method with step-by-step exploration is proposed in this article.

A. Construction Method of Node Role

It can be seen from the above analysis that it is necessary to build and change the power transfer routes according to actual requirements, and the node role should be set and changed accordingly. Therefore, the power transfer route can be switched by changing the node role. This article proposes a topology switching method to achieve this goal.

As can be seen from Fig. 2(b), the total impedance Z_i of each node N_i can be expressed as

$$Z_i = \sum Z_{fi} + R_{Li2} + j\omega L_{i2} + \frac{1}{j\omega C_{i2}} + \left(\frac{1}{j\omega C_{i1}} // \left(R_{li} + j\omega L_{i1}\right)\right). \tag{6}$$

Under the condition that the capacitances and inductances of each node satisfy (3) and (4), (6) can be simplified as

$$Z_i = \sum Z_{fi} + R_{Li2} + \frac{\left(\omega L_{i1}\right)^2}{R_{li}}. \tag{7}$$

In (7), ΣZ_{fi} is the reflected impedance from other nodes to N_i. R_{Li2} is the impedance of the coil L_{i2}, and it is very small (milliohm level). The power P_i received by N_i can be expressed as

$$P_i = \frac{U_i^2}{Z_i} \tag{8}$$

In (8), U_i is the induced voltage of N_i. Combining (7) and (8), it can be seen that if R_{li} approaches zero, ΣZ_{fi} and R_{Li2} can be ignored, Z_i will approach infinity, and P_i will approach zero. In this case, N_i does not consume power, so N_i is decoupled. Therefore, as can be seen from Fig. 2(b), if $R_{li} = 0$, S_{i3}/S_{i4} should be turned ON.

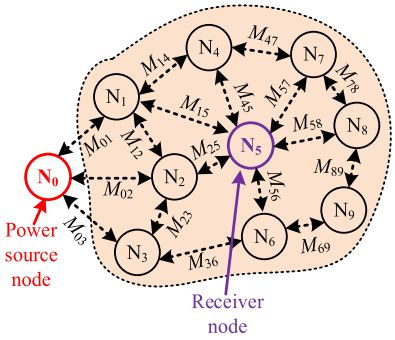

Fig. 3. WPTN with ten nodes.

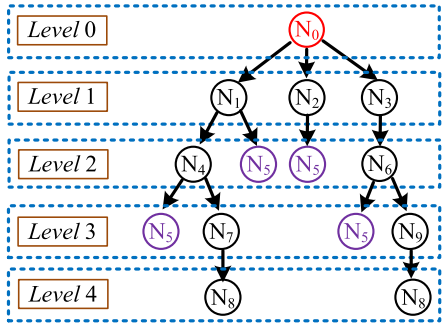

Fig. 4. Schematic diagram of node classification.

On the contrary, if R_{li} approaches infinity, $(\omega L_{i1})^2/R_{li}$ approaches zero. Because R_{Li2} is very small, Z_i can be simplified as

$$Z_i \approx \sum Z_{fi}. \tag{9}$$

Combining (8) and (9), it can be seen that N_i does not consume power itself, while the reflection impedance of other nodes on N_i consumes power. In this case, N_i acts as repeater. Therefore, as can be seen from Fig. 2(b), if $R_{li} = \infty$, the *Switch i* and S_{i3}/S_{i4} should be turned OFF. According to the above analysis, some construction rules of node role are set as follows.

1) When N_i acts as a repeater, the *Switch i* and S_{i3}/S_{i4} are turned OFF.
2) When N_i is decoupled, S_{i3}/S_{i4} are turned ON.
3) When N_i receives power, the *Switch i* is turned ON, and S_{i3}/S_{i4} are turned OFF.

B. Optimization Method of Power Transfer Route

Since the introduction of the WPTN with a large number of nodes is complicated, a WPTN with ten nodes is taken as an example to describe the route optimization method. Furthermore, this method can be applied to more nodes. The WPTN with ten nodes is shown in Fig. 3.

The optimization process of power transfer routes can be divided into three steps.

Step 1—*Explore the relative position among nodes:*

Before the start of power transmission, we do not know the position of each node. Therefore, it is necessary to explore the relative position among nodes from the power source node.

1) N_0 transmits power, and it is defined as *Level* 0.
2) When N_0 transmits power, other nodes are switched to the decoupled state to eliminate the influence of cross coupling among them, and receive power from N_0. The nodes receiving large power are considered to be strongly coupled to N_0, and they are defined as *Level* 1 (N_1, N_2 and N_3). The magnitude of power can be determined by detecting current I_{Li1}.
3) N_0 continues to transmit power, and the nodes of *Level* 1 act as repeaters in turn to explore the position of other nodes. If one node of *Level* 1 acts as repeater, the other nodes of *Level* 1 are required to be decoupled to eliminate the influence of cross coupling among them. Other nodes (N_4, N_5, N_6, N_7, N_8, and N_9) change from decoupling nodes to receiver nodes in turn to explore their coupling relationship with *Level* 1 nodes. For example, if N_1 acts as repeater, N_2 and N_3 are decoupled. Then, N_4, N_5, N_6, N_7, N_8, and N_9 change from decoupling nodes to receiver nodes in turn to explore their coupling relationship with N_1. The above process is repeated until the receiver node (N_5) receives enough large power. The magnitude of power can be determined by detecting voltage $U_{\text{out}\cdot i}$ and current I_{Li1}. The relative positions among nodes can be determined according to the above process.

Step 2—*Construct various routes from the power source node to the load node and calculate the efficiency of each route:*

According to the coupling relationships among the nodes determined in Step 1, multiple power transfer routes from N_0 to load node (N_5) can be constructed, and the efficiency in each route is calculated.

Step 3—*Select the optimal power transfer route:*

The efficiencies in different power transfer routes are compared. The route with the maximum efficiency is selected as the optimal power transfer route.

The schematic diagram of node classification and the effective power transfer route is shown in Fig. 4.

It is worth noting that when one node acts as repeater, other nodes at the same level are decoupled. For example, if N_1 acts as repeater, N_2 and N_3 are decoupled. On the one hand, the cross coupling between the nodes with strong mutual inductance is eliminated. Therefore, power can be transferred along a determined route without being bifurcated. On the other hand, this can enhance the directivity of the power transfer route from the power source node to the receiver node.

Furthermore, in the process of power transfer route extension, when the power received by a node is too low, the route will be pruned, and the power transfer route will not be extended along the node. For example, when N_0 transmits power, N_1 acts as repeater, and the power transfer route will be extended to N_4, if the power received by N_4 is too low; it proves that the mutual inductance between N_1 and N_4 is very small. Therefore, the route along N_4 will be pruned. The schematic diagram is shown in Fig. 5. According to the above method, the number of route

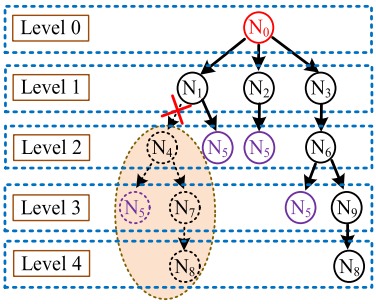

Fig. 5. Schematic diagram of power transfer route pruning.

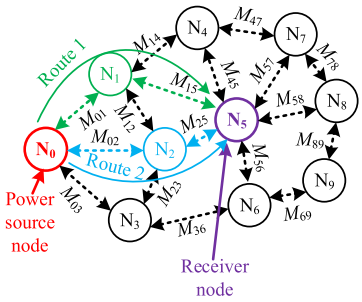

Fig. 6. Schematic diagram of two power transfer routes.

traversals can be reduced, and the route optimization time can be shortened.

C. Dynamic Switching of Power Transfer Routes

In WPTN, since the switching of power transfer route is frequent, it is necessary to study the transient variation of each node during route switching to ensure the stability in the transition process. Therefore, an example of dynamic switching of power transfer route is studied by simulation.

Schematic diagram of two power transfer routes is shown in Fig. 6. In Route 1, the power is transferred from N_0 to N_5 through the repeater N_1, and other nodes are decoupled. In Route 2, the power is transferred from N_0 to N_5 through the repeater N_2, and other nodes are decoupled. The topology of each node in different roles can refer to Table I. When the power transfer routes are switched from Route 1 to Route 2, the simulation results of transient variations of each node are shown in Fig. 7.

As can be seen from Fig. 7, in Route 1, the coil current I_{L32} of N_3 almost equal to 0. This means that the input power of N_3 is equal to 0. So N_3 does not consume power, and N_3 is decoupled. Furthermore, the coil current I_{L22} of N_2 is large enough. However, in Route 1, the topology of N_2 is L_{22}-C_{21}-C_{22}-R_{L22} in series. Under the condition of resonant state, N_2 itself consumes power only by coil resistance R_{L22}, most of the power is transferred to N_5 through N_2. Therefore, N_2 acts as repeater. Similarly, in Route 2, the power is transferred from N_0 to N_5 through the repeater N_3, and N_2 is decoupled. Furthermore, the transition process is smooth during the route switching.

TABLE I
STATE AND EQUIVALENT AC CIRCUIT OF THE NODE

N_i	*Switch i*	S_{i3}/S_{i4}	Equivalent AC circuit
Repeater node	OFF	OFF	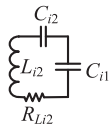
Decoupling node	—	ON	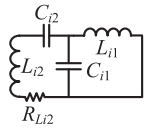
Receiver node	ON	OFF	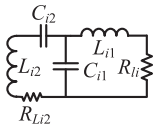

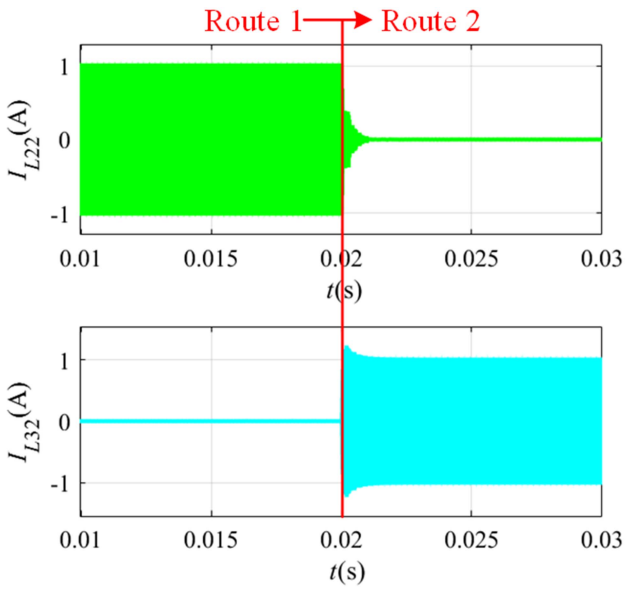

Fig. 7. Simulation results of transient variations of each node.

TABLE II
INFORMATION OF THE COIL IN THE EXPERIMENTAL SECTION

Parameter	Value	Parameter	Value
a	95 mm	*b*	145 mm
c	7 mm	wire diameter	1 mm
number of turns	30		

IV. SIMULATION AND EXPERIMENTAL VERIFICATION

An experimental demonstration platform is shown in Fig. 8. A single-chip microcomputer (STM32F103) is selected as the main control unit and MOSFET IRF540N as the main switching components. The system consists of five nodes, where N_1 is the power source node, and N_4 is the receiver node. The topology shown in Fig. 2 is adopted by each node. In the design of the experimental setup, the coil of each node is 10 cm $\times$ 15 cm rectangle. The experimental parameters are given in Tables II and III.

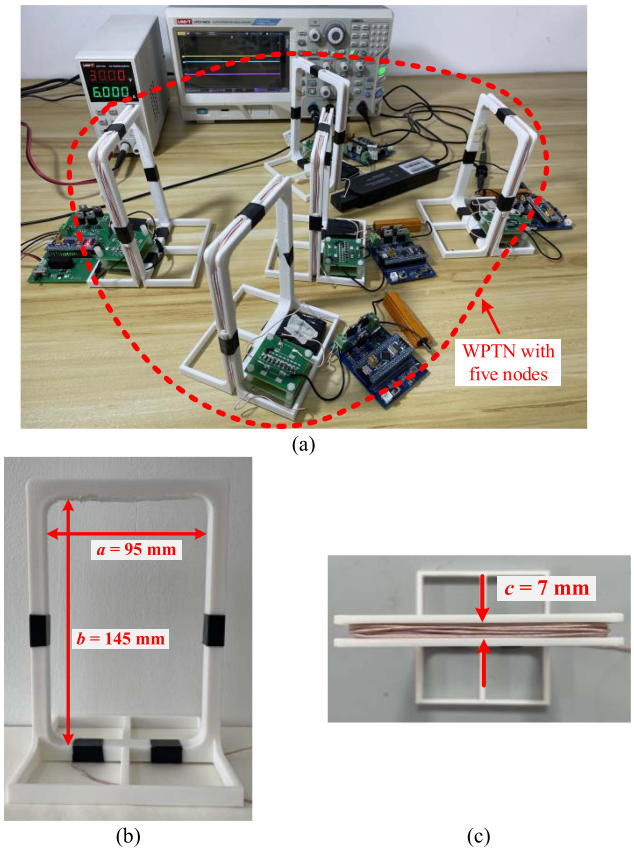

Fig. 8. Experimental setup and coil. (a) Experimental setup, (b) front view, and (c) vertical view of the coil.

TABLE III
EXPERIMENTAL PARAMETERS

Parameter	Value	Parameter	Value
U_{dc0}	30 V	f	150 KHz
L_{01}	10.93 μH	C_{01}	103 nF
C_{02}	8.94 nF	L_{02}	124.3 μH
R_{L02}	0.21 Ω	L_{11}	9.66 μH
C_{11}	116.5 nF	C_{12}	8.87 nF
L_{12}	136.6 μH	R_{L12}	0.2 Ω
L_{21}	10.13 μH	C_{21}	111.2 nF
C_{22}	9.2 nF	L_{22}	123.4 μH
R_{L22}	0.2 Ω	L_{31}	10.2 μH
C_{31}	112.6 nF	C_{32}	9.85 nF
L_{32}	124.3 μH	R_{L32}	0.21 Ω
L_{41}	10.44 μH	C_{41}	107.8 nF
C_{42}	9.88 nF	L_{42}	124.35 μH
R_{L42}	0.21 Ω		

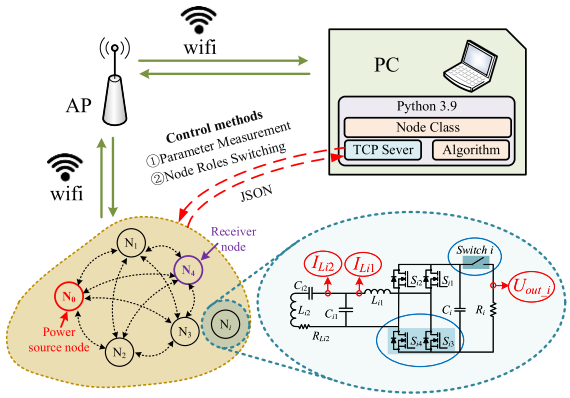

Fig. 9. Reconfiguration and optimization method of power transfer route in the experimental section.

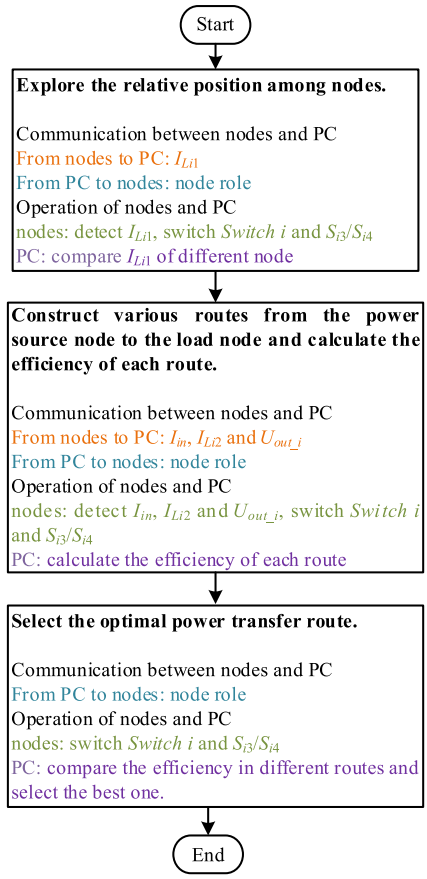

Fig. 10. Experiment steps.

The reconfiguration and optimization method of power transfer route is shown in Fig. 9 . As can be seen from Fig. 9, nodes, PC, and access point (AP) form a communication network. In certain nodes, the currents (I_{Li1} and I_{Li2}) and output voltages ($U_{\text{out}\cdot i}$) are detected, and then, they are transmitted through AP to PC via Wi-Fi in real time. Furthermore, according to the role of each node in different power transfer routes, the control signal (S_{i3}/S_{i4}) and switching signal (*Switch i*) are transmitted from PC to certain nodes through AP. Besides, the implementation steps in experimental devices are shown in Fig. 10.

In the designed WPTN, STM32F103 does not compare the advantages and disadvantages of different power transfer routes. It only collects the information of currents (I_{Li1} and I_{Li2}) and voltages ($U_{\text{out}\cdot i}$) in certain nodes in real time, and controls converters (S_{i3}/S_{i4}) and switches (*Switch i*) according to the PC instructions. The advantages and disadvantages of different power transfer routes are compared in PC.

The following will verify the effectiveness of the proposed method through simulation and experiment.

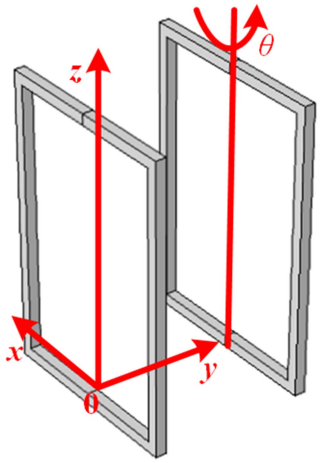

Fig. 11. COMSOL simulation model.

A. Simulation Analysis

1) Comparison and Analysis of Mutual Inductance Between Simulation and Measurement in Different Relative Distances and Angles: In the WPT system, mutual inductance is the main factor affecting the output performance of each node. Under the condition of random node distribution, the relative distances and angles among coils are the main factors affecting mutual inductance. Therefore, the node coil information shown in Fig. 8 and Table II is adopted to analyze the influence of the above two conditions on mutual inductance through COMSOL simulation software. In the COMSOL simulation model shown in Fig. 11, the relative distances are represented as x and y, and the relative angle is represented as θ. Furthermore, the simulation results are compared with the actual measurement results. The comparison results are given in Table IV and Fig. 12. The simulation and measurement results of mutual inductance are marked as S and M, respectively.

Table IV and Fig. 12 show the simulation and measurement results of mutual inductance at different relative distances and angles of coils. From the above results, it can be seen that the change trend of the actual measurement is the same as that of the simulation. Furthermore, we can see that the mutual inductance decreases with the increase of relative distances x and y. However, under different relative distances x, the variation trend of mutual inductance with respect to relative angles θ is different. It can be seen from Fig. 12(a) and (b) that under the condition that distance x is small (0 and 25), when θ increases from 0° to 90°, the mutual inductance first increases to the peak and then decreases to 0. From Fig. 12(c)–(e), we can see that under the condition that distance x is large (50, 75, and 100), the mutual inductance increases with the increase of θ.

According to the magnetic flux density method, the calculation formula of mutual inductance between single-turn rectangular coils can be expressed as

$$M = \frac{\oiint Bds}{I} \tag{10}$$

where s is the area of the receiving coil (R_X), and I is the current on the transmitting coil (T_X).

TABLE IV
SIMULATION AND MEASUREMENT RESULTS OF MUTUAL INDUCTANCE AT DIFFERENT RELATIVE DISTANCES AND ANGLES

Moving distance (mm)		S / M	M (μH)						
x	y		θ=0°	15°	30°	45°	60°	75°	90°
0	60	S	19.25	19.82	21.27	21.89	18.12	9.85	0
	100		7.59	7.70	7.90	7.80	6.66	3.93	0
	140		3.18	3.20	3.22	3.08	2.55	1.49	0
	60	M	15.01	16.25	16.86	16.73	12.85	7.03	0.05
	100		6.32	6.56	6.86	7.06	4.97	2.64	0.03
	140		2.30	2.52	2.64	2.29	2.06	1.29	0.01
25	60	S	16.80	17.30	19.00	22.36	26.40	22.61	11.36
	100		6.85	7.12	7.61	8.22	8.43	7.34	4.43
	140		2.91	3.04	3.22	3.36	3.28	2.73	1.59
	60	M	13.28	13.65	14.99	17.94	21.19	17.37	9.15
	100		5.07	5.65	6.98	7.68	8.11	6.86	3.71
	140		2.04	2.27	2.81	3.07	2.68	1.95	0.75
50	60	S	10.96	11.40	12.29	14.22	17.95	24.44	27.09
	100		4.92	5.31	5.86	6.67	7.61	8.13	7.24
	140		2.19	2.41	2.68	3.00	3.25	3.22	2.66
	60	M	8.54	8.27	8.96	10.24	13.60	20.23	23.25
	100		3.83	4.03	4.98	5.53	6.49	7.13	5.00
	140		1.48	1.76	2.05	2.56	2.93	2.64	2.06
75	60	S	4.30	5.14	5.85	6.90	8.72	11.81	16.75
	100		2.48	3.01	3.56	4.30	5.29	6.39	7.05
	140		1.23	1.52	1.83	2.21	2.63	2.95	2.94
	60	M	3.73	4.27	4.68	5.29	6.00	7.38	12.50
	100		2.35	2.59	3.02	3.98	4.85	5.12	5.87
	140		1.06	1.26	1.58	1.81	2.23	2.65	2.45
100	60	S	0.52	0.26	1.15	2.03	3.23	5.01	7.62
	100		0.27	0.89	1.44	2.08	2.92	3.98	5.05
	140		0.14	0.58	0.91	1.29	1.75	2.23	2.56
	60	M	0.43	0.30	0.91	1.86	2.55	3.83	5.39
	100		0.16	0.32	0.75	1.69	1.97	2.25	3.22
	140		0.05	0.33	0.63	1.05	1.34	2.09	2.31

In Fig. 13, the length l and width h of the receiving coil are divided into N_l parts and N_h parts, respectively, and the length and width of the small rectangle are expressed as dl and dh, respectively. Then, the mutual inductance calculation formula between single-turn rectangular coils can be expressed as

$$M|_{0\le\theta<\pi} = \frac{dldh}{I}\sum_{i=1}^{N_l}\sum_{j=1}^{N_h}|-B_{xij}\cos\theta + B_{zij}\sin\theta|. \tag{11}$$

In (11), θ is the rotation angle of the receiving coil. B_{xij} and B_{zij} are the magnetic flux density in the x-axis and y-axis directions on the small rectangle of the receiving coil, respectively.

The mutual inductance between multiturn rectangular coils can be expressed as

$$M = \sum_{m=1}^{N_T}\sum_{n=1}^{N_R} M_{mn} \tag{12}$$

where N_T and N_R are the turns of the transmitting coil and the receiving coil, respectively, and M_{mn} is the mutual inductance between the mth turn of the transmitting coil and the nth turn of the receiving coil.

It can be seen from the above analysis that the calculation of mutual inductance is complicated during the movement and rotation of the receiving coil. More detailed analysis of mutual inductance between rectangular coils is shown in [20].

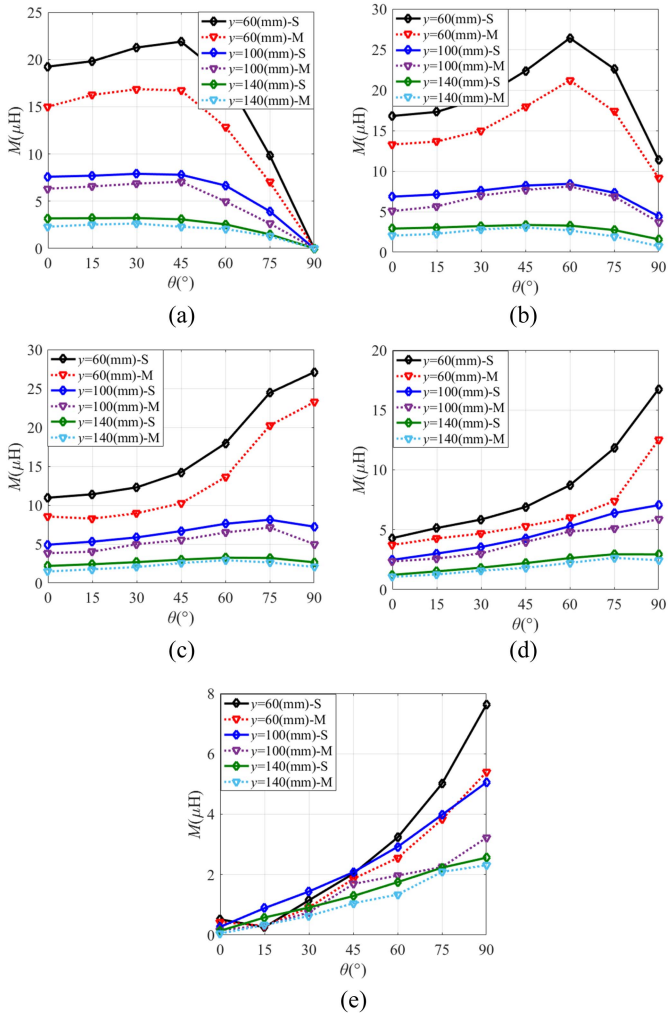

Fig. 12. Comparison of mutual inductance between simulation and measurement at different relative distances and angles of coils. (a) $x = 0$ mm, (b) $x = 25$ mm, (c) $x = 50$ mm, (d) $x = 75$ mm, and (e) $x = 100$ mm.

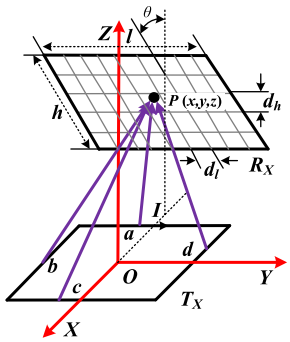

Fig. 13. Mutual inductance calculation model of single-turn rectangular coil.

2) Simulation Analysis of System Output Performance: According to the mutual inductance measurement results in Table IV, the output performance of the system will be analyzed through detailed MATLAB simulation as follows.

a) Influence of different node positions on node current in the process of node position exploration: Under the condition that each node is decoupled, when N_0 transmits power, and other

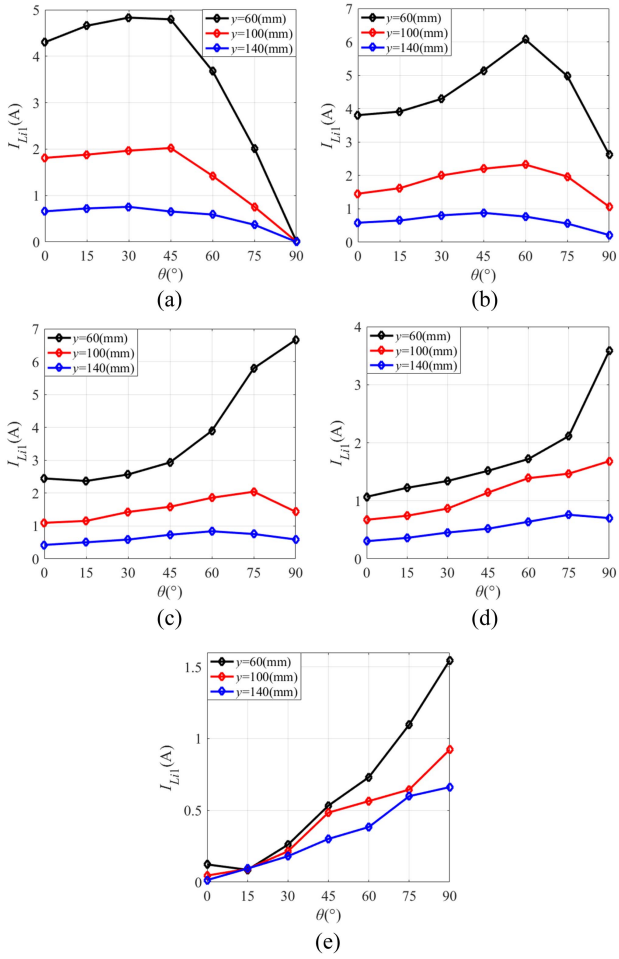

Fig. 14. Variations of current I_{Li1} at different positions of coils. (a) $x = 0$ mm, (b) $x = 25$ mm, (c) $x = 50$ mm, (d) $x = 75$ mm, and (e) $x = 100$ mm.

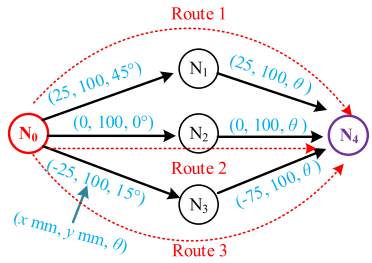

Fig. 15. Analysis model of system output performance.

nodes receives power, the variations of current I_{Li1} at different coil positions are shown in Fig. 14. From the above figures, it can be seen that the trends of current I_{Li1} and mutual inductance are the same. Therefore, the mutual inductance among nodes can be predicted by detecting the current I_{Li1}.

b) Analysis of output voltage and efficiency: It is difficult to simulate the output performance of the system under the condition of all relative distances and angles among nodes. Therefore, some typical routes are adopted to analyze the influence of different mutual inductances among nodes on system output performance. When some relative distances and angles among the nodes are fixed, as shown in Fig. 15, it can be seen

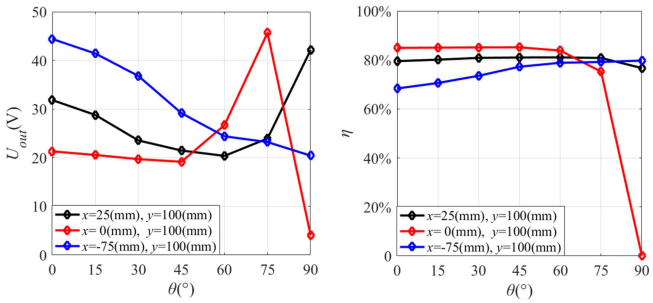

Fig. 16. System output voltages and efficiencies of N_4 at different positions. (a) Output voltages and (b) efficiencies.

from Table IV that the mutual inductances among the nodes can be expressed as: $M_{01} = 7.68\ \mu$H, $M_{02} = 6.32\ \mu$H, and $M_{03} = 5.65\ \mu$H. The simulation results of N_4 and other nodes (N_1, N_2, and N_3) at different positions are shown as follows.

When N_4 is at different positions, the output voltages U_{out} and efficiencies η of the system are shown in Fig. 16. It can be seen that the output performances (U_{out} and η) of the system are related to the node positions. Therefore, the best power transfer route can be determined by comparing the output performances on different routes.

B. Experimental Study

The validity of the theory and the feasibility of the proposed system are verified from the following aspects:

1) prediction of relative position of nodes;
2) analysis of system output performance in different power transfer routes;
3) dynamic switching of power transfer routes;
4) output performance analysis of the system without any repeaters at the same distance as Route 2;
5) analysis of system output performance under different power transfer distances in Route 2.

1) Prediction of Relative Position of Nodes: The experimental result of N_0 transmitting power and other nodes receiving power is shown in Fig. 17. I_{L11}, I_{L21}, I_{L31}, and I_{L41} are the currents of inductors L_{11}, L_{21}, L_{31}, and L_{41} in N_1, N_2, N_3, and N_4, respectively. It can be seen from Fig. 17(b) that the currents are $I_{L11} = 2.13$ A, $I_{L21} = 3.24$ A, $I_{L31} = 2.24$ A, and $I_{L41} = 0.06$ A, respectively. I_{L41} is much smaller than the others. According to the theoretical analysis, N_1, N_2, and N_3 can be defined as Level 1, and N_4 can be defined as Level 2. The prediction result of relative position of nodes is shown in Fig. 17(a).

2) Analysis of System Output Performance in Different Power Transfer Routes: The experimental results of power transfer on different routes are shown in Fig. 18, and it is summarized in Table V. U_{out} is the output voltage. I_{L12}, I_{L22}, and I_{L32} are the coil currents of N_1, N_2, and N_3 acting as repeater nodes, respectively. It can be seen from Fig. 18 and Table V that the output power in the three routes is 12.54, 59.54, and 2.21 W, respectively, and the efficiency is 64.4%, 80.6%, and 30.8%, respectively. The output power and efficiency in Route 2 are

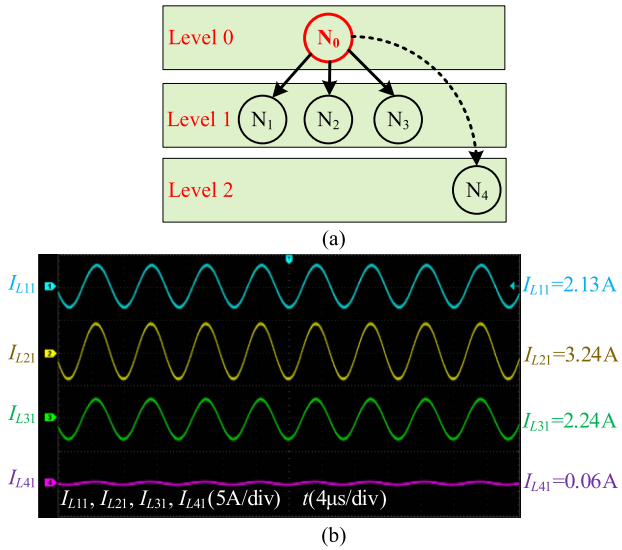

Fig. 17. Prediction of relative position of nodes. (a) Schematic diagram of node relative position prediction. (b) Experimental result.

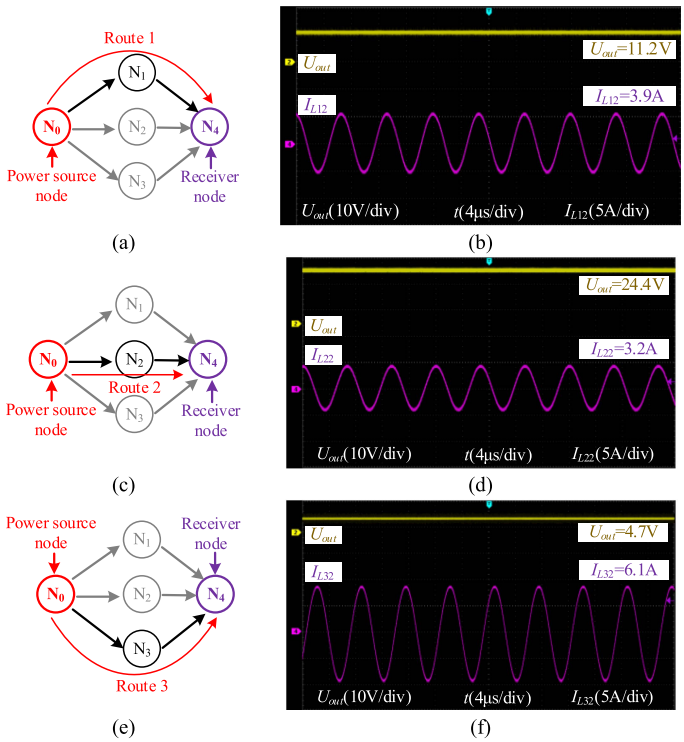

Fig. 18. Analysis of system output performance in different power transfer routes. (a) Schematic diagram and (b) experimental result in Route 1. (c) Schematic diagram and (d) experimental result in Route 2. (e) Schematic diagram and (f) experimental result in Route 3.

TABLE V
EXPERIMENTAL RESULTS

	Output voltage (V)	Output power (W)	Efficiency
Route 1	11.2	12.54	64.4%
Route 2	**24.4**	**59.54**	**80.6%**
Route 3	4.7	2.21	30.8%

The bold values indicate the optimal power transfer route.

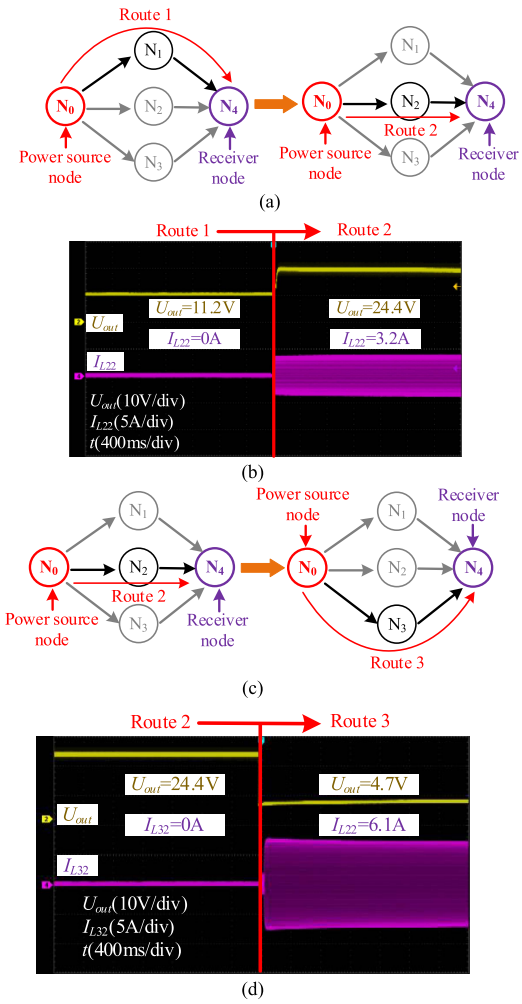

Fig. 19. Dynamic switching of power transfer routes. (a) Schematic diagram, and (b) experimental result of the power transfer route is switched from Route 1 to Route 2. (c) Schematic diagram, and (d) experimental result of the power transfer route is switched from Route 2 to Route 3.

much greater than those in other routes. Therefore, according to the theoretical analysis, Route 2 is the optimal power transfer route. In different power transfer routes, due to the significant differences of mutual inductance, high power means high efficiency.

3) Dynamic Switching of Power Transfer Routes: Dynamic switching of power transfer routes is shown in Fig. 19. It can be seen from Fig. 19(a) and (b) that when the power transfer route is switched from Route 1 to Route 2, the output voltage U_{out} changes from 11.2 to 24.4 V, and I_{L22} changes from 0 to 3.2 A. According to the theoretical analysis, N_2 is decoupled in Route 1, and it acts as repeater in Route 2. Similarly, it can be seen from Fig. 19(c) and (d) that when the power transfer route is switched from Route 2 to Route 3, the output voltage U_{out} changes from 24.4 to 4.7 V, and I_{L22} changes from 0 to 6.1 A. Therefore, N_3 is decoupled in Route 2, and it acts as repeater in Route 3. Furthermore, the transition process is smooth during the route switching.

4) Output Performance Analysis of the System Without Any Repeaters at the Same Distance as Route 2: According to the above experimental results, Route 2 is the optimal power transfer route. Under the condition that the distance between the power source node and the receiver node is the same as that on Route 2 and other nodes are removed, it can be seen from Fig. 20 that the output voltage $U_{\text{out}} = 1.5$ V. It is much smaller than that of the system with repeater nodes.

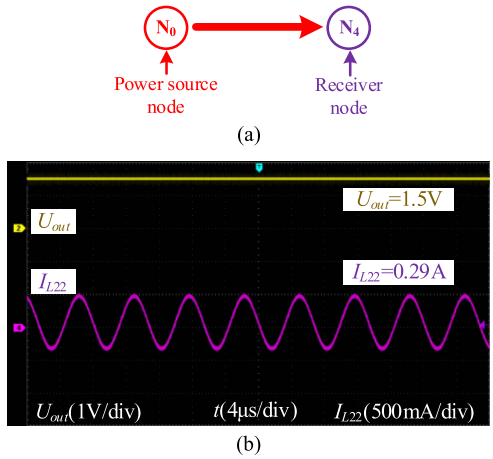

Fig. 20. System without any repeaters. (a) Schematic diagram and (b) experimental result.

5) Analysis of System Output Performance Under Different Power Transfer Distances in Route 2: According to above experimental results, Route 2 is the optimal power transfer route. The following will study the influence of changes in load and power transfer distance on output power under Route 2. It can be seen from Fig. 21(a) that the distance between N_0 and N_2 is defined as d_1, and the distance between N_2 and N_4 is defined as d_2. It can be seen from Fig. 21(b) that when the load increases from 6 to 16 Ω, P_{out} decreases from 72.9 to 51.03 W. Furthermore, it can be seen from Fig. 21(c) that when d_1 increases from 10 to 13 cm and d_2 increases from 10 to 15 cm, P_{out} varies from 77.9 to 28.62 W. P_{out} decreases with the increase of d_1, and increases first and then decreases with the increase of d_2. In Route 2, the structure of the circuit and the coupling relationships are shown in Fig. 22.

The total impedance Z_4 of N_4 can be expressed as

$$Z_4 = \frac{(\omega L_{41})^2}{R_{l4}} + R_{L42}. \tag{13}$$

The reflection impedance Z_{f4} from N_4 to N_2 can be expressed as

$$Z_{f4} = \frac{(\omega M_{24})^2}{Z_4}. \tag{14}$$

In N_0, the current I_{L02} of transmitting coil L_{02} can be expressed as

$$\dot{I}_{L02} = \frac{\dot{U}_{ac0}}{j\omega L_{01}}. \tag{15}$$

The induced voltage U_2 of L_{22} is

$$\dot{U}_2 = j\omega M_{02}\dot{I}_{L02} = \frac{\dot{U}_{ac0}M_{02}}{L_{01}}. \tag{16}$$

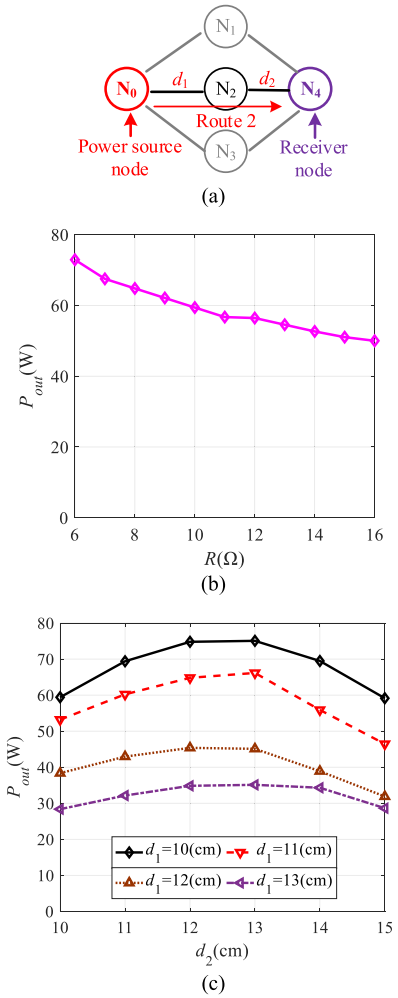

Fig. 21. Analysis of system output performance under different power transfer distances in Route 2. (a) Schematic diagram of node position, (b) the variation of the output power with load, and (c) the variation of the output power with distance.

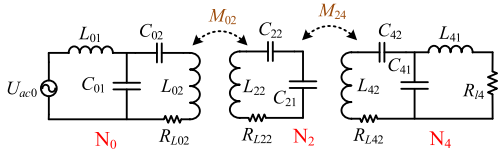

Fig. 22. Structure of the circuit and the coupling relationships between nodes in Route 2.

The current I_{L22} of L_{22} is

$$\dot{I}_{L22} = \frac{\dot{U}_2}{Z_{f4}}. \tag{17}$$

The induced voltage U_4 of L_{42} is

$$\dot{U}_4 = j\omega M_{24}\dot{I}_{L22}. \tag{18}$$

The output current I_{out} can be expressed as

$$\dot{I}_{\text{out}} = \frac{\dot{U}_4}{j\omega L_{41}}. \tag{19}$$

The output voltage U_{out} can be expressed as

$$\dot{U}_{\text{out}} = \dot{I}_{\text{out}} R_{li}. \tag{20}$$

According to (13)–(20), the output voltage U_{out} can be expressed as

$$U_{\text{out}} = \frac{U_{ac0}\omega^2 M_{02} M_{24} L_{41}}{L_{01}\left(\frac{\omega^2 M_{24}^2 R_{l4}}{(\omega L_{41})^2 + R_{l4}R_{L42}} + R_{L22}\right)\left(\frac{(\omega L_{41})^2}{R_{l4}} + R_{L42}\right)}. \tag{21}$$

If the coil resistance is ignored, U_{out} can be expressed as

$$U_{\text{out}} = \frac{U_{ac0} M_{02} L_{41}}{M_{24} L_{01}}. \tag{22}$$

It can be seen from (22) that when the load and mutual inductances change within a certain range, the output voltage U_{out} is not sensitive to load variation. Therefore, the output power P_{out} decreases with the increase of the load. In addition, U_{out} increases with the increase of M_{02}, and decreases with the increase of M_{24}. In fact, due to the influence of coil resistance on system, U_{out} increases first and then decreases with the increase of M_{24}. The variation of output power P_{out} is the same as the variation of output voltage U_{out} under the condition that the load remains constant. The experimental results are consistent with the theoretical analysis.

V. Discussion

A. Application of the Proposed Method in Electric Vehicles

In this article, one of the main contributions is that the power transfer area is extended through the power transfer routes constructed among nodes. In a WPTN composed of multiple electric vehicles, the position of load nodes (electric vehicles with power shortage) is random. Based on the dynamical node role switching method proposed in this article, the purpose of charging the load nodes at any position can be realized. And this method increases the flexibility in group electric vehicle charging. The power transfer optimization strategy can ensure the efficient transmission of power. Furthermore, the power can be shared through the coupling relationship among electric vehicles. The power can be transferred from nodes with sufficient power to nodes with insufficient power through the constructed power transfer routes, which improves the power capacity of the WPTN.

VI. Conclusion

Aiming at providing a flexible wireless power transfer mode among grouping nodes, this article proposes a wireless power transfer route method considering random node distribution. The power transfer route can be organized dynamically through node role switching. With the designed node decoupling mode, each node can be added and detached from the power transfer route flexibly. Furthermore, a topology switching strategy is put forward to realize node role switching. This route-organizing method will help to establish WPTN for group electronic devices.

REFERENCES

[1] J.-H. Cho, S. Jung, and Y.-J. Kim, "Wireless power transfer for variable load, distance, and power division ratio in a loosely-coupled multiple-receiver relay system," *IEEE Trans. Ind. Electron.*, vol. 70, no. 7, pp. 6809–6818, Jul. 2022.

[2] S. S. H. Yazdi, A. Namadmalan, A. Kapanov, A. Zollanvari, and M. Bagheri, "Optimal design of D-IPT systems considering mutual inductances and number and location of repeaters," in *Proc. IEEE Int. Conf. Environ. Elect. Eng. IEEE Ind. Commercial Power Syst. Europe*, 2022, pp. 1–6.

[3] P. Bellitti et al., "A wearable and wirelessly powered system for multiple finger tracking," *IEEE Trans. Instrum. Meas.*, vol. 69, no. 5, pp. 2542–2551, May 2020.

[4] K. E. Koh, T. C. Beh, T. Imura, and Y. Hori, "Impedance matching and power division using impedance inverter for wireless power transfer via magnetic resonant coupling," *IEEE Trans. Ind. Appl.*, vol. 50, no. 3, pp. 2061–2070, May/Jun. 2014.

[5] K. E. Koh, T. C. Beh, T. Imura, and Y. Hori, "Multi-receiver and repeater wireless power transfer via magnetic resonance coupling — Impedance matching and power division utilizing impedance inverter," in *Proc. 15th Int. Conf. Elect. Machines Syst.*, 2012, pp. 1–6.

[6] F. Zhang, S. A. Hackworth, W. Fu, C. Li, Z. Mao, and M. Sun, "Relay effect of wireless power transfer using strongly coupled magnetic resonances," *IEEE Trans. Magn.*, vol. 47, no. 5, pp. 1478–1481, May 2011.

[7] S. Y. R. Hui, W. Zhong, and C. K. Lee, "A critical review of recent progress in mid-range wireless power transfer," *IEEE Trans. Power Electron.*, vol. 29, no. 9, pp. 4500–4511, Sep. 2014.

[8] C. K. Lee, W. X. Zhong, and S. Y. R. Hui, "Effects of magnetic coupling of nonadjacent resonators on wireless power domino-resonator systems," *IEEE Trans. Power Electron.*, vol. 27, no. 4, pp. 1905–1916, Apr. 2012.

[9] Y. Zhang, T. Lu, Z. Zhao, F. He, K. Chen, and L. Yuan, "Employing load coils for multiple loads of resonant wireless power transfer," *IEEE Trans. Power Electron.*, vol. 30, no. 11, pp. 6174–6181, Nov. 2015.

[10] C. Cheng, W. Li, Z. Zhou, Z. Deng, and C. Mi, "A load-independent wireless power transfer system with multiple constant voltage outputs," *IEEE Trans. Power Electron.*, vol. 35, no. 4, pp. 3328–3331, Apr. 2020.

[11] W. Zhong and S. Hui, "Auxiliary circuits for power flow control in multifrequency wireless power transfer systems with multiple receivers," *IEEE Trans. Power Electron.*, vol. 30, no. 10, pp. 5902–5910, Oct. 2015.

[12] X. Shu, B. Zhang, Z. Wei, C. Rong, and S. Sun, "Extended-distance wireless power transfer system with constant output power and transfer efficiency based on parity-time-symmetric principle," *IEEE Trans. Power Electron.*, vol. 36, no. 8, pp. 8861–8871, Aug. 2021.

[13] X. Hou, Y. Su, Z. Zuo, X. Dai, and Y. Fei, "A novel analysis method based on quadratic eigenvalue problem for multirelay magnetic coupling wireless power transfer," *IEEE Trans. Power Electron.*, vol. 36, no. 9, pp. 9907–9917, Sep. 2021.

[14] W. Zhong, C. Lee, and S. Hui, "Wireless power domino-resonator systems with noncoaxial axes and circular structures," *IEEE Trans. Power Electron.*, vol. 27, no. 11, pp. 4750–4762, Nov. 2012.

[15] W. Zhong, C. K. Lee, and S. Y. R. Hui, "General analysis on the use of Tesla's resonators in domino forms for wireless power transfer," *IEEE Trans. Ind. Electron.*, vol. 60, no. 1, pp. 261–270, Jan. 2013.

[16] J. Lee and K. Lee, "Effects of number of relays on achievable efficiency of magnetic resonant wireless power transfer," *IEEE Trans. Power Electron.*, vol. 35, no. 7, pp. 6697–6700, Jul. 2020.

[17] J. Wu, X. Dai, and R. Gao, "A coupling mechanism with multidegree freedom for bidirectional multistage WPT system," *IEEE Trans. Power Electron.*, vol. 36, no. 2, pp. 1376–1387, Feb. 2021.

[18] J. Wu, X. Dai, and Y. Sun, "A node role dynamic change method among repeater, receiver, and decoupling using topology switching in multinode WPT system," *IEEE Trans. Power Electron.*, vol. 36, no. 10, pp. 11174–11182, Oct. 2021.

[19] F. Farajizadeh, D. M. Vilathgamuwa, P. Jayathurathnage, and G. Ledwich, "Graph sets method for multicoil wireless power transfer systems—Part I: Principles," *IEEE Trans. Power Electron.*, vol. 35, no. 10, pp. 10741–10756, Oct. 2020.

[20] Z. Li, J. Li, S. Li, Y. Yu, and Y. J, "Design and optimization of asymmetric and reverse series coil structure for obtaining quasi-constant mutual inductance in dynamic wireless charging system for electric vehicles," *IEEE Trans. Veh. Technol.*, vol. 71, no. 3, pp. 2560–2572, Mar. 2022.

Jinde Wu received the B.S. degree in automation with the College of Information Engineering, Taiyuan University of Technology, Taiyuan, China, in 2015, and the Ph.D. degree in control theory and control engineering from the School of Automation, Chongqing University, Chongqing, China, in 2021.

He is currently with the College of Electrical and Power Engineering, Taiyuan University of Technology. His research interests include wireless power transfer, computer vision, intelligent sensor, and detection technology.

Yanling Li received the Ph.D. degree in control theory and control engineering from the School of Automation, Chongqing University, Chongqing, China, in 2017.

She is currently with the School of Electrical Engineering and Electronics Information, Xihua University, Chengdu, China. Her current research interests include wireless power transfer and advanced control technology in power electronics.

Xin Dai (Member, IEEE) received the B.S. degree in industrial automation from Yuzhou University, Chongqing, China, in 2000, and the Ph.D. degree in control theory and control engineering from the School of Automation, Chongqing University, Chongqing, in 2006.

In 2012, he was a Visiting Scholar in The University of Auckland, Auckland, New Zealand. He is currently a Professor with the School of Automation, Chongqing University. His current research interests include inductive power transfer technology and nonlinear dynamic behavior analysis of power electronics.

Ruozhong Gao (Student Member, IEEE) received the B.S. and M.Sc. degrees in electrical engineering from the Taiyuan University of Technology, Taiyuan, China, in 2013 and 2017, respectively. He is currently working toward the Ph.D. degree in control theory and control engineering with Chongqing University, Chongqing, China.

His current research interests include the wireless power transfer and power electronics.

Miao He (Senior Member, IEEE) received the B.S. degree from Nanjing University of Posts and Telecommunications, Nanjing, China, in 2005, the M.S. degree from the Tsinghua University, Beijing, China, in 2008, and the Ph.D. degree from Arizona State University, Tempe, AZ, USA, in 2013, all in electrical engineering.

In 2013, he joined the faculty of Texas Tech University, Lubbock, TX, USA, where he is currently an Associate Professor with the Department of Electrical and Computer Engineering. His research interests include deep learning applied to modeling, control, and optimization of smart grids, power networks, and renewable energy.